Iraqi Journal of Science, 2026, Vol. 67, No. 4, pp: 2457- 2471
DOI: 10.24996/ijs.2026.67.4.43

ISSN: 0067-2904

Mineralogy, Geochemistry, and Laboratory Spectroscopic Study of Plasma Generated around Meteorites using an Nd: YAG Laser

Abdullah K. Ahmed[1], Waleed Ibrahim Yaseen[1]*, Harth E. Al-Jubury[2]
[1]*Department of Astronomy and Space, College of Science, University of Baghdad, Baghdad, Iraq*
[2]*Department of Geology, College of Science, University of Baghdad, Baghdad, Iraq*

Received: 30/10/2024 Accepted: 14/ 4/2025 Published: 30/4/2026

Abstract

Meteorites are a crucial subject that assists in comprehending the components of the solar system. They burn entirely or partially when they enter the atmosphere due to friction. A plasma will generate surroundings and finally a mass ablation. By studying the spectrum of the forming plasma around them, we can investigate the chemical compositions of the meteorites' mass and the parameters of the plasma. In this work, a laboratory study was conducted on a genuine meteorite that fell in the city of Baghdad. A sample was taken from the meteorite and bombarded with a laser to obtain plasma. Optical emission spectroscopy was used to diagnose plasma parameters using the Boltzmann method and LIBS (Q-switched Nd: YAG pulsed laser). A vacuum chamber was used to experiment under a working pressure of 0.1 mbar. Additionally, laser energies ranged from 600 mJ to 1000 mJ, and a Thorlabs spectrometer with an operating range of 320 nm to 740 nm were used. Plasma parameters were calculated using atomic iron Fe I various peaks. The electron temperature, density, length of Debye, and plasma frequency rose in the meteorite surrounding plasma as a response to the laser energy increase.

For the mineralogical composition, meteorite samples have a simple silicate composition. The minerals found were diopside pyroxene (augite), serpentine talc, and secondary magnetite. The main composition is lazurite, which is mainly composed of fine-crystalline grains that directly replace the olivine grains.

Keywords: LIBS technique, Meteorite, Boltzmann methods, plasma parameters, chemical composition.

دراسة المعادن والجيوكيمياء والتحليل الطيفي المعملي للبلازما المتولدة حول النيازك باستخدام ليزر Nd: YAG

عبد الله كامل احمد[1], وليد ابراهيم ياسين*[1], حارث اسماعيل مصطاف الجبوري[2]
[1]*قسم الفلك والفضاء, كلية العلوم, جامعة بغداد, بغداد, العراق*
[2]قسم علم الارض, كلية العلوم, جامعة بغداد, بغداد, العراق

الخلاصه

النيازك موضوع بالغ الأهمية يساعد في فهم مكونات النظام الشمسي. تحترق النيازك كليًا أو جزئيًا عند دخولها الغلاف الجوي بسبب الاحتكاك. ستولد البلازما محيطًا وأخيرًا تآكلًا كتليًا. من خلال دراسة طيف البلازما المتكونة حولها، يمكننا التحقيق في التركيب الكيميائي لكتلة النيازك ومعامِلات البلازما. في هذا العمل، أجريت دراسة معملية على نيزك حقيقي سقط في مدينة بغداد. تم أخذ عينة من النيزك وقصفها بالليزر

*Email: waleedib1972cnc@gmail.com

للحصول على البلازما. تم استخدام مطيافية الانبعاث الضوئي لتشخيص معلمات البلازما باستخدام طريقة بولتزمان و LIBS ليزر Nd: YAG النبضي Q-switched .تم استخدام غرفة فراغ للتجربة تحت ضغط عمل 0.1 ملي بار. بالإضافة إلى ذلك، تتراوح طاقات الليزر من 600 ملي جول إلى 1000 ملي جول، ومطياف Thorlabs بمدى تشغيل من 320 نانومتر إلى 740 نانومتر. تم حساب معلمات البلازما باستخدام ذرات الحديد Fe I المختلفة. ترتفع درجة حرارة الإلكترون وكثافته وطول ديباي وتردد البلازما في النيزك المحيط بالبلازما استجابة لزيادة طاقة الليزر.

بالنسبة للتركيب المعدني، تحتوي عينات النيزك على تركيبة سيليكات بسيطة. المعادن الموجودة هي البيروكسين الديوبسيدي (الأوجيت)، والتالك السربنتيني، والمغنتيت الثانوي. التركيب الرئيسي هو اللازورديت، والذي يتكون بشكل أساسي من حبيبات بلورية دقيقة تحل محل حبيبات الزبرجد مباشرة.

1.Introduction

Laser induced breakdown spectroscopy (LIBS) is used for quantitative and qualitative elemental analysis of liquids gases and solid materials [1]. A method of atomic emission spectroscopy called laser induced breakdown spectroscopy (LIBS) employs heated vaporization dissolution and excitation from laser generated breakdown plasma [2]. The approach has various advantages the most significant of which is the ability to interrogate material in situ and remotely without any pretreatment since focused optical light forms plasma [3, 4]. A laser induced plasma (LIP) is shaped onto or into the sample light is collected from the plasma and then it is analyzed spectroscopically to accomplish LIBS measurement [2]. This technique is crucial for space research comet and meteorite identification and surface analysis on planets. Space agency projects about Mars exploration have recently shown a significant deal of interest in using LIBS to investigate the rocks and soils of some planets like Mars [5, 6]. Understanding the origin and evolution of a planetary body is of primary importance for LIBS to know the chemical composition of crustal materials like rocks and dust [7] [8]. Meteorites which are thought to be igneous rocks that originated on Mars were examined. Since Martian meteorites are thought to be accreted rocks and contain substantially higher levels of sopholevene, they have been researched intensively to give possible petroleum limitations on Mars's geological history [9]. Cosmo chemists have often examined fluffy cometary dust by examining Interplanetary Dust Particles (IDPs) in a lab setting. Meteor spectroscopy which focuses on the light released during the process of ablation and breakup of these particles in the atmosphere owing to their high-velocity contact with the Earth is another profession that studies this subject. Meteor spectroscopy offers intriguing insights into the chemical makeup of approaching meteoroids and the ablation process [10, 11]. The Local Thermodynamic Equilibrium (LTE) assumption and a range of values related to element ratios serve as the foundation for the study and the ensuing categorization. The line width, or Boltzmann plot indicates the excitation temperature in the plasma created by the falling meteorite, which changes with distance from the solid body and ranges from 0.86 to 0.43 eV [12]. It is clear that the accuracy of this approach depends only on the choice of the examined emission lines and the method used to determine the population's composition from the stimulated [13]. In the LIBS laboratory, a series of tests were run on a meteorite sample to confirm the viability of LIBS for meteorite analysis validate the standard procedure used for object measurements in flight, and choose more suitable spectral lines for elemental analysis given the available laboratory resolution. Ferus et al. conducted experimental studies to interpret meteorite spectra and determine the elemental composition of meteorites using the calibration-free LIBS technique. A LIBS chemical study of meteorites was presented by Ciucci et al., Tognoni et al., Del Aglio et al., and Takahashi et al. [14]. Meteorites are derived from 100–150 asteroids [15] as well as from the Moon and Mars [16] and possibly from comets [17]. Micrometeorites are derived mostly from asteroids [18]. Achondrite meteorites are defined by a lack or deficiency of chondrules

and are dominated by silicate mineral assemblages, according to the current classification of meteorites [19]. The composition of stony meteorites (chondrite meteorites) includes two principal molecules namely, magnesium orthosilicate, Mg_2SiO_4, olivine with an isomorphic admixture of ferrous orthosilicate, and magnesium metasilicate, MgSiOs with varying amounts of added ferrous metasilicate (the rhombic pyroxene series) [20]. The meteorite used in this study was found in Baghdad Sadr Al-Qanat area. It consisted of three pieces: two large pieces and the other small. One piece was found visible and the rest was buried at a depth of about 10 cm approximately a year ago. The spectroscopic technique was used to study the elements that made up the meteorite as well as to study the plasma formed around the meteorite model used and to calculate the plasma parameters using the Boltzmann method and Lorenz expansion. Chemical analysis was used to determine the elements and chemical composition of the meteorite.

2. Emission Spectroscopy Studies

Optical emission spectroscopy technology is used to diagnose plasma and determine its composition. A Thorlab spectrometer was used to record the whole spectrum, and the lines that were released were measured between 320 and 740 nm in length. Spectral light naturally enters the entrance aperture of the spectrometer through an optical fiber containing a lens to focus the light. The intensity of the atomic emission lines the spectrometer produces is used to calculate the excitation temperature of the electron and species that are reactive. Using the NIST database, the transition probability values and statistical weight can be extracted [21]. The electron temperature is determined from spectroscopic data using the Boltzmann plot method [22, 23].

$$\ln\left(\frac{I_n\lambda_n}{g_nA_n}\right) = C - \frac{E_n}{KT_e} \quad (1)$$

Where E_n, k, λ_n, g_n, T_e, and I_n, represent upper-level energy, Boltzmann constant, wavelength, statistical weight for level n, electron temperature, and Intensity, respectively; An is the coefficient of transition probability. In this experiment, the constant C is very low and, therefore, is presented as zero. Plotting the logarithm term of several lines of emission in the equation versus E_n allows for the observation of their relative strengths. The slope of the straight line is equal to $1/kT_e$. Thus, obtaining T_e is simple from Eq. (1) [24]. Electrons traveling quickly and ions moving more slowly form electrical fields that affect the emission species (atoms or ions) in plasma. Stark broadening, a phenomenon wherein atoms or ions experience a shift in their energy levels due to the perturbing electrical field, is a resultant broadening of plasma emission lines. Utilizing the spectrum widths of the Stark-broadening emissions line can calculate the electron density. Rather than Doppler and collisional broadening or instrumental broadening, the Stark-widening effect dominates the spectral line width in our scenario. The full width at half maximum (FWHM) of the Stark-broadened line determines the electron density, which is determined by [25, 26]:

$$\Delta\lambda_{1/2} = 2\omega\left(\frac{n_e}{10^{16}}\right) \quad (2)$$

Where n_e is electron number density (cm^{-3}), and ω is the electron impact width parameter. The impact factor ω is taken from Konjevic, et.al. 2002 [27].

There are many parameters used to characterize the plasma such as Debye length (λ_D), which is calculated as follows [28]:

$$\lambda_D = \sqrt{\frac{\varepsilon_o KT_e}{e^2\, n}} \quad (3)$$

Where (ε_o) is the permittivity of free space, e is electron charges its constant ($1.6x10^{-19}$), and m_e is electron mass. Plasma frequency ω_p can be calculated as [29]:

$$\omega_p = \sqrt{\frac{n_e e^2}{\varepsilon_o m_e}} \tag{4}$$

$$f_p = 8.89\sqrt{n_e} \tag{5}$$

where ne is the electron density and fp is the linear plasma frequency.

3. Materials

The system used in this work consists of a Q-switched Nd:YAG pulsed laser spectroscopic system, system (vacuum chamber and rotary pump),as shown in Figure 1.

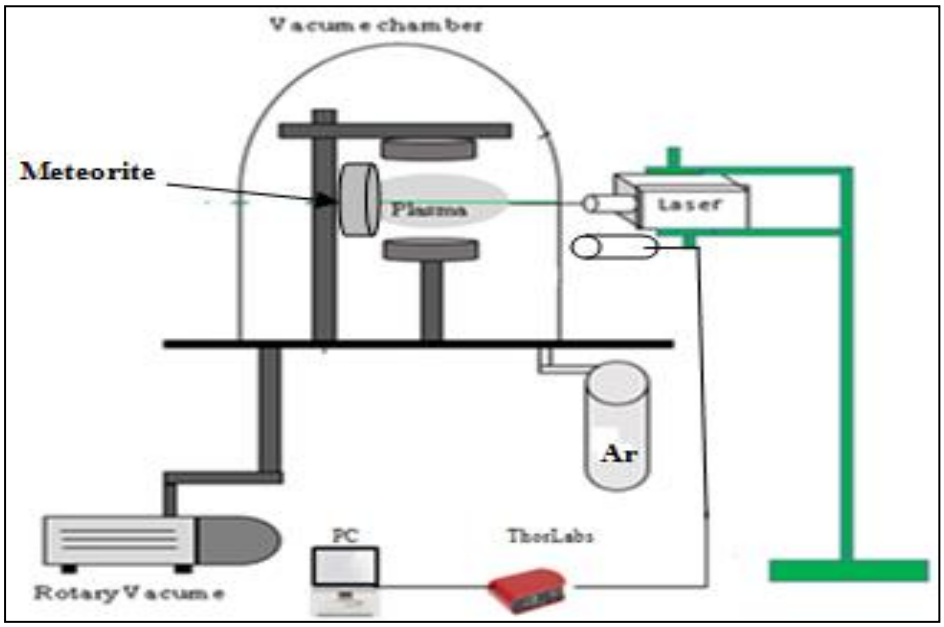

Figure 1: Setup vacuum system Q-switched Nd:YAG pulsed laser, spectroscopic system, a vacuum system, and a target holder..

A meteorite model was used as a target with a diameter of 2 cm and a thickness of 1 cm and was fixed to one side of the vacuum chamber. Light emission from the plasma generated as a result of meteorite bombardment was detected using an Ocean Optics (hr-4000 cg-UVNIR) spectrometer in the range 320 nm to 740 nm. In this work, a sample of dimensions of 5 x 3 cm was taken from a chondrite meteorite that fell in Baghdad, Sadr Al-Qanat, as shown in Figure 2.

Figure 2: Sample of chondrite meteorite that fell in Baghdad, Sadr Al-Qanat

4. Results and Discussion

Optical Emission Studies

The iron meteorite's spectrum was measured between 321 and 750 nm. The NIST spectrum database was used to identify the spectral lines for the components listed in Table 1 [30]. Figure 3 displays the spectrum lines of the elements found in the LIBS spectrum of the iron meteorite.

The unique ability of LIBS to identify both heavy and light components is a clear benefit. There were many peaks in the range from 320 nm to 740 nm; there were some atomic FeI peaks: (381.8, 632.1, 674.1, and 734.7) nm in meteorite samples (358.1, 364.7, 371.9, 373.4, 374.5, 375.8, 382.0, 385.9, 404.5, 406.3, 432.5, and 438.3) nm.

Table 1: Physical parameters required for the calculation of the Boltzmann method of the 12 atomic lines for different elements in the recorded spectra of the iron meteorite.

λ (nm)	Intensity (a.u) at P=600 mJ	Intensity (a.u) at P=800 mJ	Intensity (a.u) at P=900 mJ	Intensity (a.u) at P=1000 mJ	g.A	E_k (eV)
Fe I 358.1	0.0124	0.024	0.0398	0.0469	2.58E+08	6.696
Fe I 364.7	0.0183	0.0352	0.0506	0.0751	1.01E+08	6.4695
Fe I 371.9	0.0137	0.0131	0.0133	0.016	3.62E+07	6.0919
Fe I 373.4	0.0584	0.0862	0.127	0.17246	2.43E+08	6.258
Fe I 374.5	0.0377	0.0583	0.0868	0.1102	1.63E+08	6.306
Fe I 375.8	0.0325	0.0561	0.0803	0.11422	2.48E+07	6.59967
Fe I 382.0	0.0632	0.1	0.14	0.1989	7.20E+08	6.51085
Fe I 385.9	0.0212	0.0624	0.0547	0.1128	3.55E+07	6.42699
Fe I 404.5	0.0752	0.124	0.176	0.249	6.08E+07	6.30606
Fe I 406.3	0.609	0.101	0.144	0.203	1.70E+07	6.47908
Fe I 432.5	0.078	0.128	0.178	0.246	5.29E+06	6.13237
Fe I 438.3	0.111	0.176	0.251	0.348	1.69E+07	6.40132

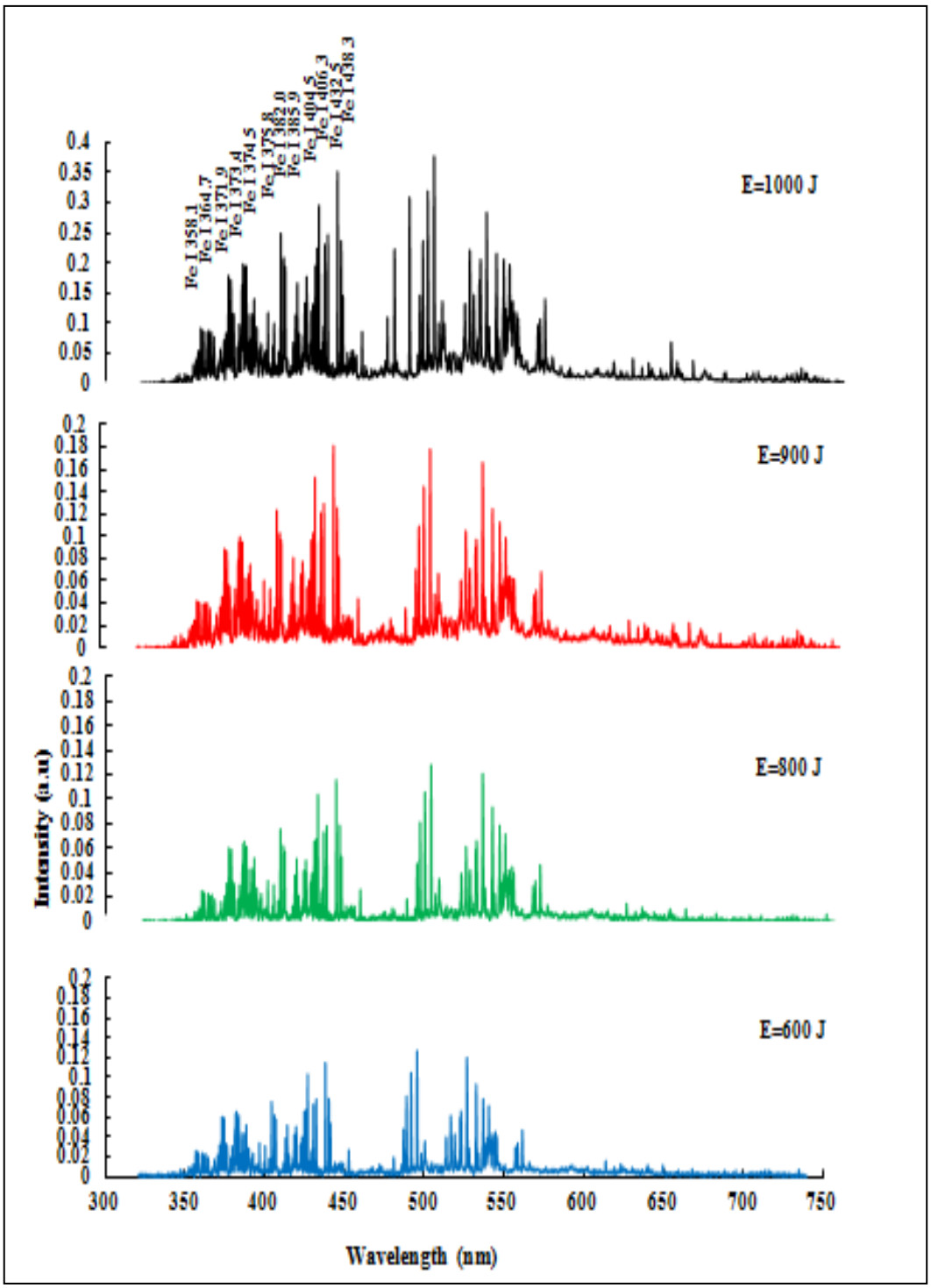

Figure 3: Typical laser-induced breakdown spectroscopy (LIBS) spectra of iron meteorite in the wavelength range 321-750 nm for different laser energy (600, 800, 900, and 1000 mJ).

The electron temperature (T_e) is the primary determinant of the many forms of excitation and ionization in plasma. The electron temperature is determined by considering that the plasma is in the LTE state and that the number of ionized atoms inside the plasma is dependent on Boltzmann distribution. The value of T_e is calculated according to Eq. (1) with data listed in Table 1. For the determination of the electron temperature, a graph of $\ln(I\lambda/gA)$ vs. E_k is drawn, and a Boltzmann plot is constructed, as illustrated in Figure 4.

The Boltzmann diagram is one of the most widely used methods for determining the electron temperature in various types of plasma.

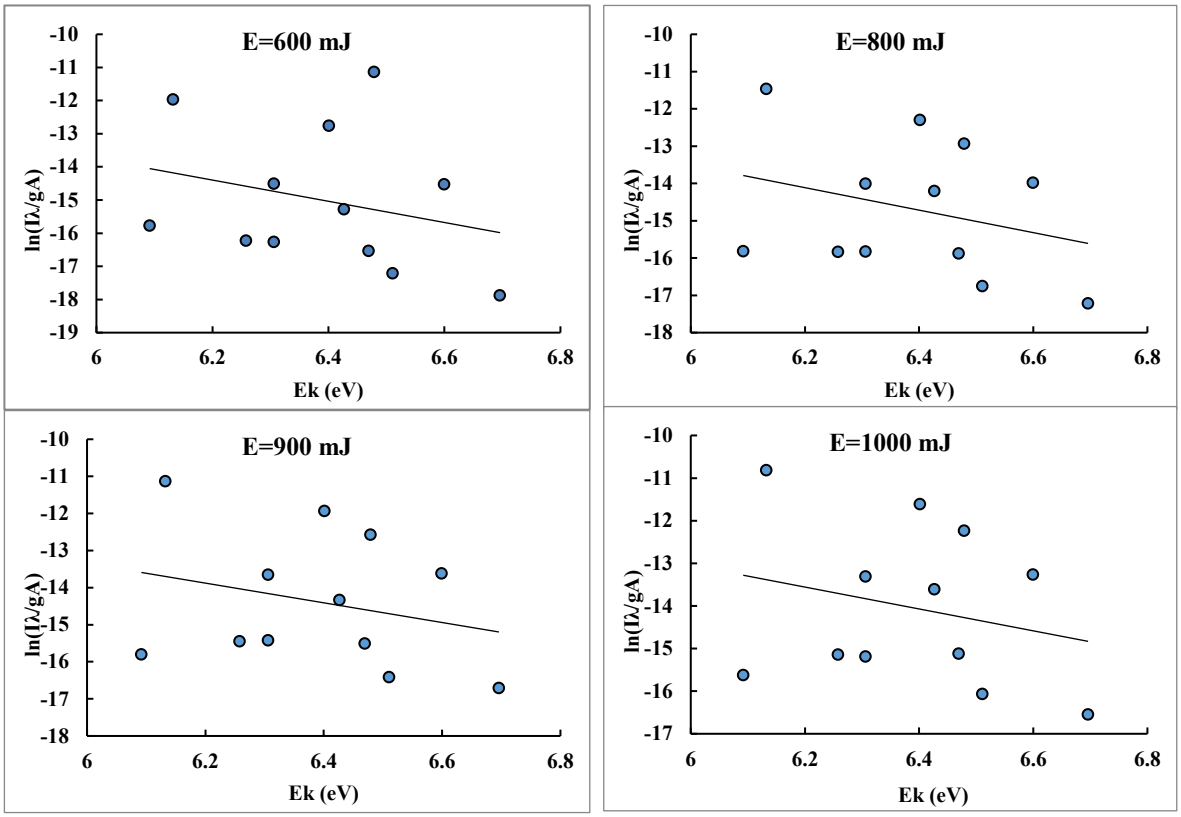

Figure 4: Boltzmann plot for different laser energy (600, 800, 900, and 1000 mJ) for Iron meteorite.

The effect of pulse laser energy on the electron temperature can be illustrated in Figure (5). The results in this figure indicate a positive relationship between electron temperature and laser energy. The high electron temperature seen close to the meteorite surface may be the result of absorbing more radiant energy during the laser pulse contact. These results agree with Rashid et al. [31].

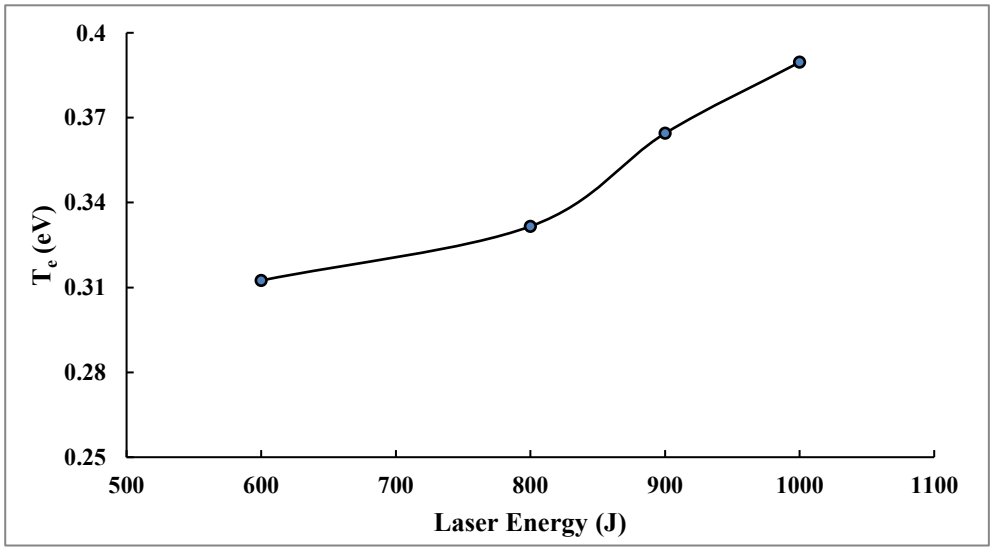

Figure 5: Electron temperature vs. Laser energy for iron meteorite.

It is possible to calculate the average of the electrons number density the laser-induced plasma by determining the full width at half-maximum (FWHM), of the Fe I 438.3 nm Stark-broadened line, as shown in Figure 6.

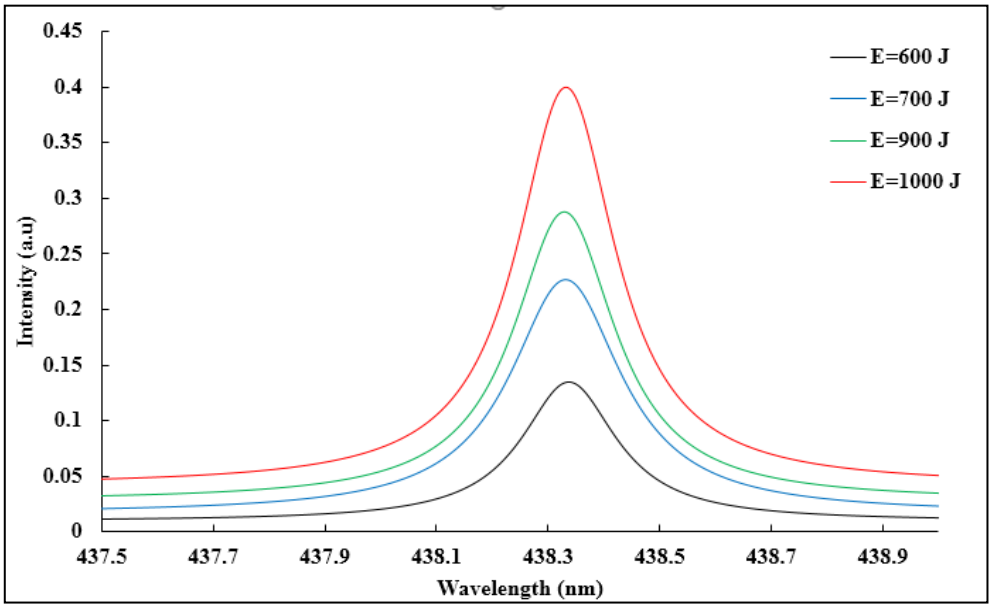

Figure 6: Measured and fitted Lorentzian of the Fe I 438.3 nm line of the iron meteorite.

Figure 7 illustrates the behavior of the electron density at the various laser energy values investigated in this study. It can be seen that for energies between 600 and 1000 mJ, the electron density rises by laser energy, from 1.5 x10^{16} m^{-3} to 1.63 x10^{16} m^{-3}.

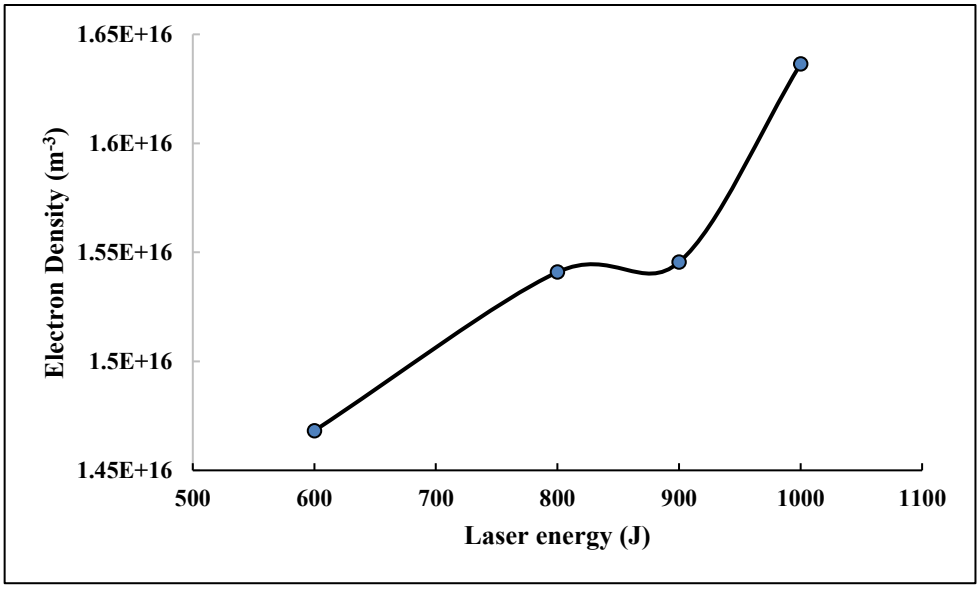

Figure 7: Electron density vs. Laser energy for iron meteorite.

This behavior of the ne is explained by the laser energy being absorbed or reflected by the plasma during creation, depending on the frequency it may be expressed as a decreased plasma frequency relative to the laser frequency, which is regarded as an energy loss in practical applications, may also suggest that raising the laser's irradiance leads to the

production of more excited species, ions, and free electrons. These species then interact with the laser pulse, which causes more heating and ionization. This allows for a greater utilization of the incoming laser energy. Inverse Bremsstrahlung absorption and photoionization are the two primary absorption mechanisms known to occur during plasma production. Our results agree with other studies, including Abdellatif and Imam [32], and Hanif [33]. Figure 8 displays the Debye shielding length of plasma in a vacuum medium produced by Nd: YAG laser irradiation as a function of pulse laser energy. The Debye length is related to the electron density and temperature, where it varies inversely with ne and directly with Te. It is clear that the Debye length has the largest value at high energy. The Debye length is larger at high energy because the electron temperature is lower. The plasma frequency in the vacuum laser-induced plasma for the meteorite component target is displayed in Figure 8. It is evident from the graphic that as the laser peak power increases, so does the plasma frequency, these results agree with [34].

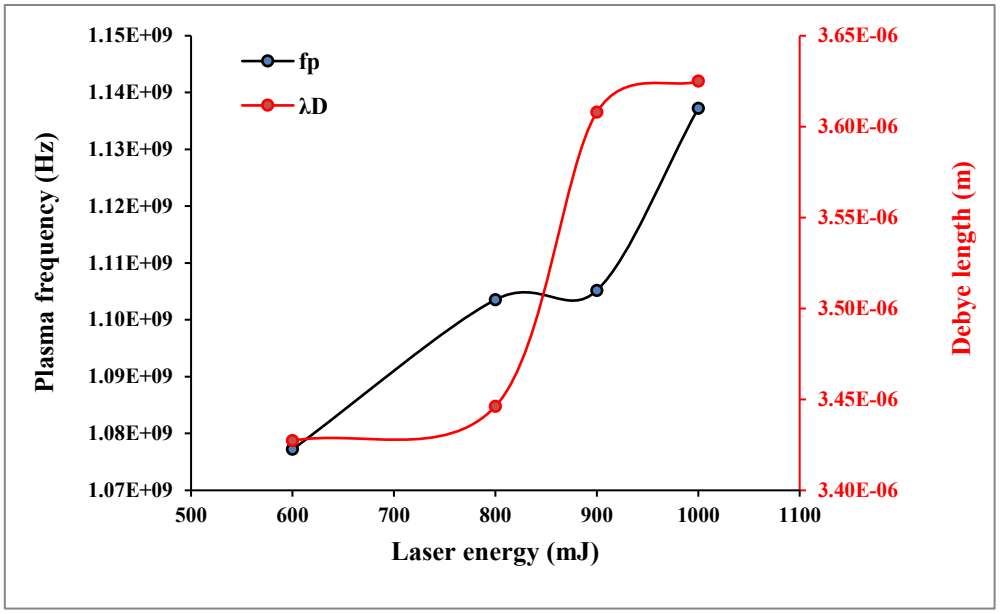

Figure 8: Debye length and plasma frequency vs. Laser energy for iron meteorite.

Mineralogy

After preparing thin sections of the meteorite sample for the purpose of studying it mineralogically, it was found that the sample consists of the metamorphosed serpentine mineral, resulting from the decomposition process of ultramafic rocks, which are mainly composed of olivine mineral (Figure 9), and the deformed pyroxene mineral as a result of metamorphic processes (Figure 9). The Talc mineral was also found, which is a mineral produced through the decomposition process of ultramafic rocks in the form of veins surrounding the serpentine mineral (Figure 10).

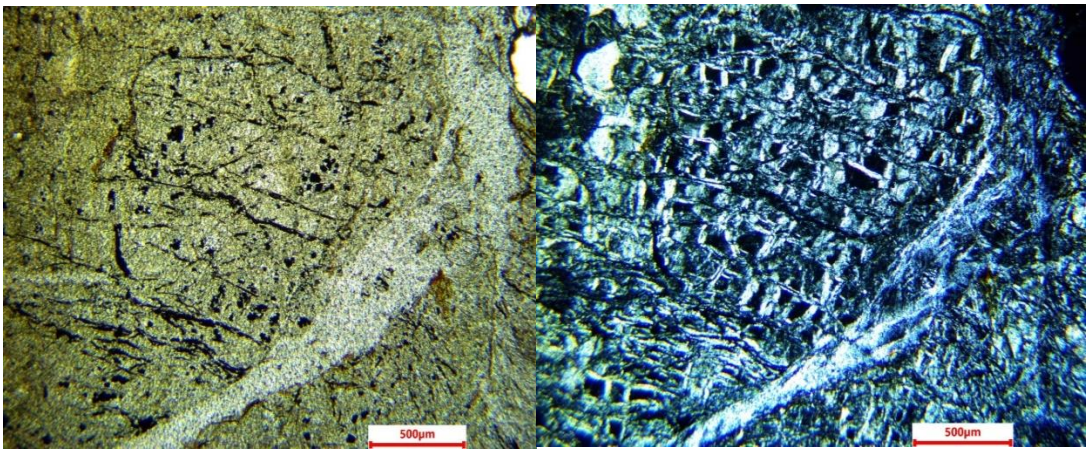

Figure 9: Mesh textured serpentine with veins of talc and secondary magnetite.

The secondary magnetite mineral was also observed in the form of veins and clusters that fill the voids and vugs in the serpentine mineral which result from the process of ionic replacement between the elements Mg and Fe through the exchange process between the original minerals of the ultramafic rocks and hydrothermal solutions, which are considered the main factor in the decomposition processes of the original rocks.

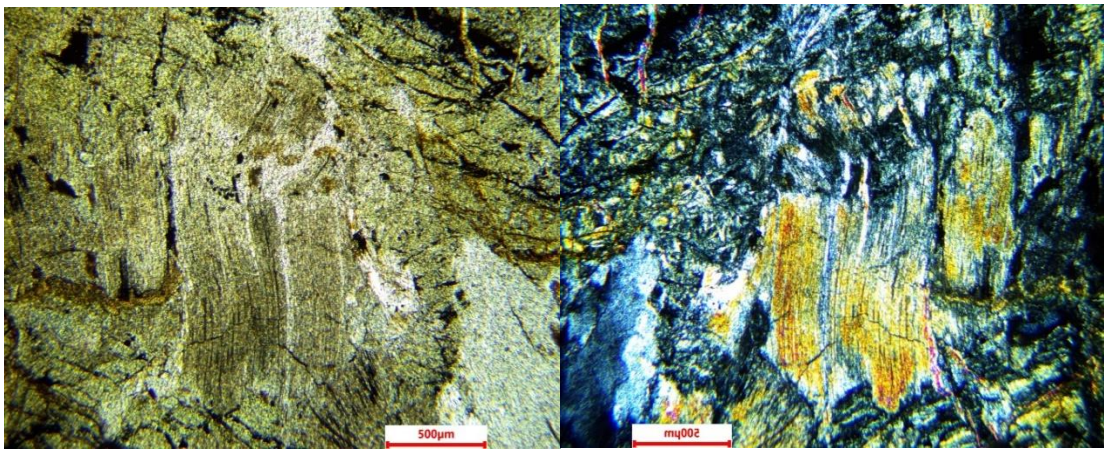

Figure 10: Serpentinized deformed pyroxene in a serpentinite.

These solutions subtract the Mg element into the rock and gain the Fe element, which leads to changing the original minerals of the ultrabasic rock (olivine mineral and pyroxene mineral) to serpentine mineral with secondary iron veins [35].

Based on the XRD (X-ray diffraction) analysis of the meteorite sample illustrated in Figure 11 it is evident that the primary mineral composition of the studied rock sample is lizardite. Lizardite is prominently present as fine crystalline grains that have directly replaced the olivine grains within the rock. This replacement process is significant because it indicates retrograde metamorphism specifically within the context of serpentine minerals. Retrograde metamorphism refers to the mineralogical changes that occur in rocks as they are subjected to decreasing temperature and pressure conditions often resulting in the formation of new minerals.

Lizardite is one of the serpentine minerals which are typically formed from the alteration of magnesium rich silicate minerals such as olivine and pyroxene. The presence of lizardite in the meteorite sample suggests that the rock has undergone significant metamorphic transformations. The XRD analysis reveals the presence of secondary magnetite within the

rock. Magnetite is an iron oxide mineral that commonly forms as a secondary mineral during the alteration of primary minerals [35].

The occurrence of secondary magnetite in the meteorite sample indicates that the rock has experienced alteration or metamorphism involving fluid interactions. These interactions likely introduced iron into the rock leading to the formation of magnetite. The combination of lizardite and secondary magnetite in the sample provides valuable insights into the geological history and metamorphic processes that have affected the meteorite.

In summary the XRD analysis highlights that the main mineral in the meteorite sample is lazurite which has replaced olivine grains, signifying the retrograde metamorphism of serpentine minerals. The presence of secondary magnetite further indicates that the rock has undergone alteration involving fluids that introduced iron into the system. These findings offer a detailed understanding of the mineralogical and metamorphic history of the meteorite sample.

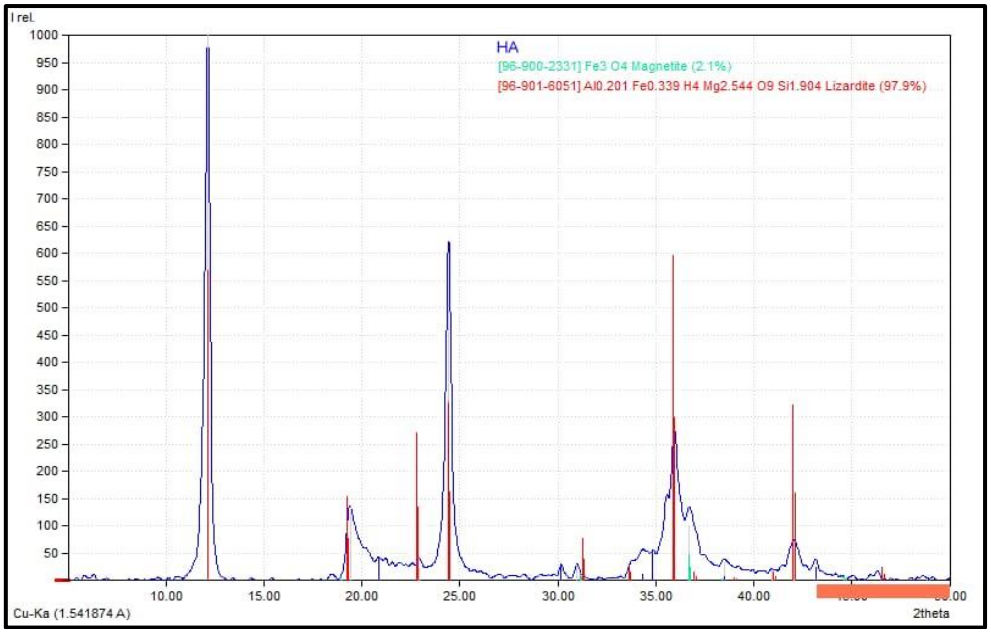

Figure 11: X-ray diffractogram of sample HA

Geochemistry

From the results of the chemical analysis of the meteorite sample, it is clear to us that the percentage of MgO is high (42.87%), as shown in Table 2, due to the strong influence of the serpentinization process on the original content of the original rock (ultramafic) compared to other oxides [35]. It was also observed that the percentage of SiO_2 increased, amounting to 45.11%, and this, in turn, indicates the progress and increase of the serpentinization process of the original rock.

Table 2: Representative ICP-MS analysis major (wt.%) of sample HA.

Oxides %	Sample HA
SiO_2	45.11
TiO_2	0.0346
Al_2O_3	1.0618
Fe_2O_3	9.265
MnO	0.1320
MgO	42.87
CaO	1.175
Na_2O	0.0775
K_2O	0.00043
Cr_2O_3	0.2761
Total	100

The CaO content (1.175%) in serpentinite can be attributed to several factors: the original rock composition, and the nature of the fluid phase derived from the slab due to its relative solubility of calcium in the aqueous fluids interacting with the edge of the slab. The Al_2O_3 value (1.0618%) of the sample may indicate that the serpentinite is derived from the remains of the jibbah. The results of the chemical analysis show a low Na_2O content (0.0775%) of the serpentinite due to both metasomatism and mechanical mixing between the metabolic masses and the processes of the serpentinite matrix. The high percentage of Fe_2O_3 (9.265%) indicates progress in the serpentinization process. This transformation likely occurs under low-grade metamorphic conditions within the stability domain of serpentine. This result indicates regressive metamorphic conditions, as substantial changes in iron oxidation must occur near the exotic masses during the metamorphic process [36]. The percentage of TiO_2 (0.0346%) indicates the high content of TiO_2 in serpentinite by mechanical mixing due to dilution by SiO_2 enrichment and the addition of H_2O [37]. The percentage of K_2O (0.00043%) indicates progress in the serpentinization process and an increase in the water-fluid interaction during the serpentinization process of the original model. The percentage of MnO (0.1320%) indicates the immobility of MnO during serpentinization processes.

Conclusions

By studying the mineralogy of the meteorite sample, it becomes clear that the sample is a metamorphic rock of the serpentinite type (chondrite), which could be formed by the infiltration of water poor in carbon dioxide into the original ultramafic rocks. From this, it can be concluded that the environment in which the meteorite sample was formed is similar to one of the environments that form this type of rock on the surface of the Earth, which is either in a mid-ocean ridge, mountain forces, or subduction zones.

The results of the following geochemical analysis show: the high influence of the serpentinization process on the original content of the original rock (ultramafic) by the percentage of MgO and the increase of SiO_2. The sample may indicate that the serpentinite is derived from the remains of the jibbah. The high percentage of Fe_2O_3 indicates progress in the serpentinization process. This transformation likely occurs under low-grade metamorphic conditions within the stability domain of serpentine. This result indicates regressive metamorphic conditions, as substantial changes in iron oxidation must occur near the exotic masses during the metamorphic process. The percentage of K_2O indicates progress in the

serpentinization process and an increase in the water-fluid interaction during the serpentinization process of the original model.

Meteorite spectroscopy can be used as a valuable tool to determine the chemical quantities of meteorites and calculate the electron temperature and electronic density of the plasma generated around the meteorite using a pulsed laser. Using meteorite spectroscopy to deduce plasma parameters in meteorites has enabled us to conclude that increasing the laser energy leads to an increase in the electron temperature and an increase in the electronic density, length of Debye, and plasma frequency of the plasma generated around the meteorite, and this is what happens when the meteorite penetrates the Earth's gaseous atmosphere, where its temperature increases as a result of the force of air restraint, which increases ionization of the air surrounding the meteorite, through the large number of iron peaks and the high concentration of Fe_2O_3 in the meteorite used, which was confirmed by geochemical analysis. It can be concluded that the meteorite is susceptible to magnetization and magnetic attraction.

References

[1] K. A. Aadim, "Characterization of Laser induced cadmium plasma in air," Iraqi Journal of Science, vol. 56, no. 38, pp. 2292-2296, 2015.

[2] D. A. Cremers and L. J. Radziemski, History and fundamentals of LIBS, New Yourk: National University of Kaohsiung, 2018.

[3] S. Palancoa, J. Baenab and J. Lasernaa, "Open-path laser-induced plasma spectrometry for remote analytical measurements on solid surfaces," Spectrochimica Acta , vol. 57, p. 591–599, 2002.

[4] D. A. Cremers, "The Analysis of Metals at a Distance Using Laser-Induced Breakdown Spectroscopy," Applied Spectroscopy, vol. 41, no. 4, pp. 572-579, 1987.

[5] A. K. Knight, N. L. Scherbarth, D. A. Cremers and A. M. J. Ferris, "Characterization Of Laser-Induced Breakdown Spectroscopy (Libs) For Application To Space Exploration," Applied Spectroscopy, Vol. 54, No. 3, pp. 331-340, 2000.

[6] S. K. Sharma, P. G. Lucey, M. Ghosh, H. W. Hubble and K. A. Horton, "Stand-off Raman spectroscopic detection of minerals on planetary surfaces," Spectrochimica Acta, vol. 59, pp. 2391-2407, 2003.

[7] F. Colaoa, R. Fantonia, V. Lazica, A. Paolinia, F. Fabbria, G. Orib, L. Marinangelib and A. Balivab, "Investigation of LIBS feasibility for in situ planetary exploration:An analysis on Martian rock analogues," Planetary and Space Science , vol. 52, p. 117 – 123, 2004.

[8] B. Salle´, D. A. Cremersb, S. Mauricec, R. C. Wiensd and P. Fichete, "Evaluation of a compact spectrograph for in-situ and stand-off Laser-Induced Breakdown Spectroscopy analyses of geological samples on Mars missions," Spectrochimica Acta, vol. 60, p. 805 – 815, 2005.

[9] L. A. Taylor, M. A. Nazarov, C. K. Shearer, H. Y.Mcsween, J. Cahill, C. R. Neal, M. A. Ivanova, L. D. Barsukova, R. C. Lentz, R. N. Clayton And A. T. K. Mayeda, "Martian Meteorite Dhofar 019: A New Shergottite," Meteoritics & Planetaryscience , Vol. 37, Pp. 1107-1128, 2002.

[10] J. M. Trigo-Rodriguez, J. Llorca, J. Borovi»Ka And A. J. Fabregat, "Chemical Abundances Determined From Meteor Spectra: I. Ratios of The Main Chemical Elements," Meteoritics & Planetary Science, Vol. 38, No. 8, P. 1283–1294 , 2003.

[11] J. M. Trigo-Rodrıguez, J. Llorca and J. Fabregat, "Chemical abundances determined from meteor spectra – II. Evidence for enlarged sodium abundances in meteoroids," Mon. Not. R. Astron. Soc., vol. 348, p. 802–810, 2004.

[12] Pavol Matlovi, Adriana Pisar číková1, Veronika Pazderová1, Stefan Loehle, Juraj Tóth, Ludovic Ferrière, Peter Cermák, David Leiser, Jérémie Vaubaillon, and Ranjith Ravichandran, "Spectral properties of ablating meteorite samples for improved meteoroid composition diagnostics", Astronomy & Astrophysics preprint, pp. 1-19, 2024.

[13] K. Chaudhary, S. Z. H. Rizvi and a. J. Ali, "Laser-Induced Plasma and its Applications," Plasma Science and Technology, pp. 260-273, 2016.

[14] M. Ferus, P. Kubelík, L. Petera, L. Lenža, J. Koukal, A. Kˇrivková, V. Laitl, A. Knížek, H. Saeidfirozeh, A. Pastorek, T. Kalvoda, L. Juha, R. Dudžák, S. Civis, E. Chatzitheodoridis and a. M. Krus, "Main spectral features of meteors studied using a terawatt-class high-power laser," Astronomy and Astrophysics, vol. 630, no. 127, pp. 1-20, 2019.

[15] Burbine; T.J. Mcoy; A. Meibom; B. Gladman; K. and Keil, "Meteoritic Parent Bodies: Their Number and Identification. In: Bottke Cellino, J.W.F.A., Paolicchi, P., Binzel, R.P. (Eds.), Asteroids III," The University of Arizona Press, Tucson, p. 653–667, 2002.

[16] Shearer, P. J.J. and R. F.J.M., "The planetary sample suite and environments of origin. In Planetary Materials. In: Papike, J.J. (Ed.), Reviews in Mineralogy," Mineralogical Society of America, Washington, pp. 1-28, 1998.

[17] Gounelle, S. P. and B. P.A., "The orbit and atmospheric trajectory of the Orgueil meteorite from historical records," Meteorit. Planet. Sci., vol. 41, pp. 135-150, 2006.

[18] Kurat; C. Koeberl; T. Presper; B. Franz; and Maurette, M., "Petrology and geochemistry of Antarctic micrometeorites," Geochim. Cosmochim. Acta, vol. 58, p. 3879–3904, 1994.

[19] M. Weisberg, M. T. J. and K. A. N., "In Meteorites and the Early Solar System II, ed. D. S. Lauretta & H. Y. McSween," Jr. Tucson, AZ: Univ. Arizona Press, vol. 19, 2006.

[20] Vinogradov and V. G. P., "The Composition of Meteorites," Geokhimiya, vol. 715, no. 8, 1963.

[21] A. Kramida, Y. Ralchenko and a. J. Reader, "Atomic Spectra Database," 2017.

[22] R. B. Tyata1, D. P. Subedi, R. Shrestha and A. C. S. Wong, "Generation of uniform atmospheric pressure argon glow plasma by dielectric barrier discharge," Pramana Indian Academy of Sciences, vol. 80, no. 3, p. 507–517, 2013.

[23] Waleed Ibrahim Yaseen, Ala F. Ahmed, Duraid A. Al-Shakarchi, Falah A.-H. Mutlak, "Development of a high power LC circuit for generating arc plasma and diagnostic via optical emission spectroscopy," Applied Physics A, vol. 128, no. 148, pp. 2-9, 2022.

[24] A. S. Wasf, H. R. Humud and M. E. Ismael, "Spectroscopic measurements of the electron temperature in low pressure microwave 2.45 GHz argon plasma," Iraqi Journal of Physics, vol. 13, no. 27, pp. 14-23, 2015.

[25] H. R. Humud and a. S. Hussein, "Optical emission spectroscopy for studying the exploding copper wire plasma parameters in distilled water," Iraqi Journal of Physics, vol. 15, no. 35, pp. 142-147, 2017.

[26] N. Shaikh, B. Rashid, S. Hafeez, Y. Jamil and a. M. Baig, "Measurement of electron density and temperature of a laser-induced zinc plasma," J Phys D Appl Phys, vol. 39, pp. 1384-1391, 2006.

[27] N. Konjevic, A. Lesage, J. R. Fuhra and …. a. W. L. Wiese, "Experimental Stark Widths and Shifts for Spectral Lines of Neutral and Ionized Atoms," J. Phys. Chem. Ref. Data, vol. 31, no. 3, pp. 819-925, 2002.

[28] A. A.-K. Hussain, K. A. Aadim and W. I. Yaseen, "Diagnostics of low-pressure capacitively coupled RF discharge argon pl8asma," Iraqi Journal of Physics, 2015 Vol.13, No.27, PP., vol. 13, no. 27, pp. 76-82, 2015.

[29] A. Aseel Kamel and Q. A. Abbas, "Spectral Analysis of the Effects of Variation in Electrodes' Area forDielectric Barrier Discharge Actuator," I raqi Journal of Science, vol. 64, no. 4, pp. 1691-1703, 2023.

[30] "https://physics.nist.gov/PhysRefData/ASD/lines_form.html".

[31] B. Rashid, S. Hafeez, N. Shaikh, M. Saleem, R. Ali and a. M. Baig, "Diagnostics of copper plasma produced by the fundamental, second and third harmonic of a ND:YAG laser," Int J Modern Phys, vol. 21, pp. 2697-2710, 2007.

[32] G. Abdellatif and a. H. Imam, "A study of the laser plasma parameters at different laser wavelengths," Spectrochim Acta B, vol. 57, pp. 1155-1165, 2002.

[33] M. Hanif, M. Salik and a. M. A. Baig, "Spectroscopic studies of the laser produced lead plasma," Plasma Sci.Technol., vol. 13, no. 2, 2011.

[34] Ruaa K. Hassan, and Mohanad A. Aswad, "Study the Plasma Parameters due to the Different Energies for Laser Produced Lead Oxide Plasma," Indian Journal of Natural Sciences, vol. 10, no. 57, pp. 17908-17914, 2019.

[35] E. H. Al-Jubury, M. Y. T. Agha and A. M. Aqrawi, "Petrography and Geochemical Relationships of the Ultramafic Rocks in Galalah area within Erbil Governorate, NE Iraq," Iraqi Journal of Science, vol. 64, no. 1, pp. 228-252, 2023.

[36] I. Parkinson and a. J. Pearce, "Peridotites from the Izu-Bonin-Mariana forarc (ODP Leg 125): Evidence for mantle melting and melt- mantle interaction in asuprasubduction zone setting," Jour. of Petrology, vol. 39, pp. 1577-1618, 1998.

[37] R. King, J. Mattew and a. J. Eiler, "Constraints on the petrologic structure of the subduction zone slab-mantle interface from Franciscan Complex exotic ultramafic blocks," GSA Bulletin, vol. 115, pp. 1097-1109, 2003.